A microfluidic model for single-cell capillary obstruction by *Plasmodium falciparum*-infected erythrocytes

J. Patrick Shelby*, John White†, Karthikeyan Ganesan*, Pradipsinh K. Rathod*†‡§, and Daniel T. Chiu*‡

Departments of *Chemistry and †Pathobiology, Box 351700, University of Washington, Seattle, WA 98195-1700; and §Seattle Biomedical Research Institute, Seattle, WA 98109

Edited by George M. Whitesides, Harvard University, Cambridge, MA, and approved October 14, 2003 (received for review June 26, 2003)

Severe malaria by *Plasmodium falciparum* is a potentially fatal disease, frequently unresponsive to even the most aggressive treatments. Host organ failure is associated with acquired rigidity of infected red blood cells and capillary blockage. *In vitro* techniques have played an important role in modeling cell deformability. Although, historically they have either been applied to bulk cell populations or to measure single physical parameters of individual cells. In this article, we demonstrate the unique abilities and benefits of elastomeric microchannels to characterize complex behaviors of single cells, under flow, in multicellular capillary blockages. Channels of 8-, 6-, 4-, and 2-μm widths were readily traversed by the 8 μm-wide, highly elastic, uninfected red blood cells, as well as by infected cells in the early ring stages. Trophozoite stages failed to freely traverse 2- to 4-μm channels; some that passed through the 4-μm channels emerged from constricted space with deformations whose shape-recovery could be observed in real time. In 2-μm channels, trophozoites mimicked "pitting," a normal process in the body where spleen beds remove parasites without destroying the red cell. Schizont forms failed to traverse even 6-μm channels and rapidly formed a capillary blockage. Interestingly, individual uninfected red blood cells readily squeezed through the blockages formed by immobile schizonts in a 6-μm capillary. The last observation can explain the high parasitemia in a growing capillary blockage and the well known benefits of early blood transfusion in severe malaria.

Plasmodium falciparum is responsible for ≈1–2 million deaths every year; severe malaria is typically characterized by brain, spleen, liver, or kidney pathology (1–3; see also www.who.int/inf-fs/en/fact094.html). The severity of *P. falciparum* infection is a function of capillary blockage by infected cells in these organs. Normal erythrocytes are highly deformable liquid-filled compartments (4). They owe their high degree of deformability to low internal viscosity, high surface-area-to-volume ratio, and the highly elastic nature of the erythrocyte membrane and underlying cytoskeleton (2). Particularly during the late stages of parasite development, infected erythrocytes become spherocytic, develop knob-like structures, and lose their native deformability. This loss of deformability is often cited as an important contributing factor in capillary blockage (5).

Given the complications of *in vivo* testing and the lack of a relevant animal model (1), a number of physical approaches have been applied to the study of deformability of infected red blood cells (RBCs), usually on bulk cell populations (6). In pioneering studies, the higher pressures required to pass malaria-infected blood in comparison with normal blood through a polycarbonate filter suggested that infected erythrocytes lacked structural deformability, which in turn contributed to capillary blockage (7, 8). In addition, viscometers, after correction for hematocrit, provided information about the viscosity of erythrocytes (7, 9). Ektacytometry, using diffraction patterns from erythrocytes illuminated with a He-Ne laser in a highly viscous medium such as dextran, provided measurements of erythrocyte deformability in bulk medium (5, 10). Expanding on the concept of filtration, the single erythrocyte rigidometer (SER) (11, 12) characterizes the time of passage of a single erythrocyte through a micrometer-sized pore (e.g., 5.8 μm); thus, cell area, volume, and cytoplasmic viscosity were determined. The SER technique has been applied to the study of the physical properties of normal erythrocytes. The rheoscope, which uses fluid shear stress to visualize erythrocyte physical characteristics, allowed study of erythrocyte deformability and the tank tread-like motion of the erythrocyte membrane (13). The rheoscope has been used to characterize the deformability of *P. falciparum*-infected erythrocytes and the recovery of RBCs in the ring stage of infection (14). Micropipette aspiration improved studies on the deformability of a single cell and measurement of membrane viscoelasticity and rigidity (15, 16). The time required for entry, time constant for extensional recovery, and the critical pressure required to aspirate an erythrocyte into a 3- to 3.5-μm diameter pipette have been determined for malaria-infected erythrocytes. Now microfluidics offers opportunities to study properties of single infected-erythrocytes, in real time, in a capillary-like microenvironment.

Microfluidic devices have found numerous applications in biology, biochemistry, and medicine because of their ability to efficiently control and replicate microenvironments (17, 18). They also offer practical benefits such as limiting human exposure to large amounts of biohazardous samples. Microfluidic systems are easy to fabricate, owing to recent advancements in rapid prototyping, and provide an ideal environment for testing either bulk samples or single entities, such as individual cells. Recognizing the need for devices that mimic the capillary microenvironment, many researchers have designed capillary-like channel systems in silicon[¶] (19–22) and glass (23) substrates. The ability to fabricate micrometer-sized features in glass and silicon makes these materials attractive options for making capillary-sized structures. Through these studies, it has been possible to record normal erythrocyte area, volume, and deformability. Many of these devices are integrated into comprehensive test platforms with controlled flow rate, temperature, and pressure. This advance enabled researchers to develop systems that closely mimic the *in vivo* environment. Although providing a geometrically similar environment to capillaries, silicon and glass channels do not have structural properties, such as elastic modulus, of capillary tissue. Recently, structural information of normal erythrocytes was determined by using a human erythrocyte microchannel analyzer made in a silicone elastomer (24). In the present study, we apply similar microfluidic techniques to the study of malaria-infected erythrocytes.

This paper was submitted directly (Track II) to the PNAS office.

Abbreviations: RBC, red blood cell; PDMS, poly(dimethylsiloxane).

‡To whom correspondence should be addressed. E-mail: rathod@chem.washington.edu and chiu@chem.washington.edu.

¶Kikuchi, Y., Ohki, H., Kaneko, T. & Sato, K. (1989) *Biorheology* **26,** 1055 (abstr.).

www.pnas.org/cgi/doi/10.1073/pnas.2433968100

Materials and Methods

Fabrication of Microchannels. Fabrication of test channels in poly-(dimethylsiloxane) (PDMS) used rapid prototyping (25). Briefly, a high-resolution chrome mask (Photosciences, Inc., Torrance, CA) was generated from a computer-aided drawing file and etched by an electron beam. The mask was a negative of the channel design and was used in contact photolithography with SU-8 photoresist (MicroChem, Newton, MA) to create a negative "master," which consisted of bas-relief features of SU-8 on a silicon wafer. From the master, PDMS channels were molded and then sealed irreversibly to a borosilicate glass coverslip by oxidizing the PDMS surface in oxygen plasma, which also caused the channels to become hydrophilic. Access holes to the channels were formed by using a punch made from a 21-gauge needle. Polyethylene tubing (PE20) was then inserted into the access holes, which were slightly smaller than the outer diameter of the tubing, to form a pressure seal between the tubing and the hole. The tubing was attached to a 3-ml syringe through which fluid was introduced into the channel. The length of the constricted portion of the channel was designed to be ≈3 to 5 times its width. The depth of all channels was restricted to 2 μm to prevent the disk-shaped erythrocytes from turning on their sides and traversing the constriction.

***P. falciparum*-Infected Erythrocytes.** *P. falciparum* parasites were maintained under standard conditions (26) in a 2% suspension of human A+ erythrocytes in complete medium (RPMI medium 1640 supplemented with 20% human A^+ serum; GIBCO/Invitrogen). Mixed-stage parasite cultures were synchronized by two consecutive sorbitol treatments (27) and harvested for analysis at the ring stage (0–6 h postsync), early trophozoite stage (16–21 h postsync), late trophozoite stage (21–24 h postsync), and schizont stage (36–42 h postsync). Giemsa staining of thin smears showed >95% purity of the synchronized cultures. Each cell culture sample contained ≈1% of infected erythrocytes.

Cell Visualization. The test samples were mounted onto a Nikon TE300 microscope with a Nikon ×100 Superfluar objective (numerical aperture = 1.3) for bright-field, differential interference contrast, and fluorescence imaging. A high-sensitivity black and white charge-coupled device camera (Cohu, San Diego, CA) was used to capture images. While differential interference contrast imaging readily identified infected erythrocytes, some infected cultures were stained with 2′,7′-bis-(2-carboxyethyl)-(5 and 6)-carboxyfluorescein acetoxymethyl ester (BCECF-AM) (Molecular Probes) by using published methods (28). Fluorescent images were obtained by exciting the stained cells with the 488-nm line of a continuous wave Ar^+ ion laser (Spectra-Physics). To prepare the suspension of infected RBCs for flowing through the microchannels, ≈0.5-ml culture solution (2% hematocrit and 1% parasitemia) was diluted in ≈0.5-ml of complete RPMI medium 1640. The temperature of the sample above the objective was 25°C. The velocity in the 20-μm main channel for each experiment was ≈50 $\mu m \cdot s^{-1}$, and the velocities in the constriction varied from ≈125 $\mu m \cdot s^{-1}$ in the 8-μm channel to ≈500 $\mu m \cdot s^{-1}$ in the 2-μm channel, which resulted in a pressure drop across the restriction of ≈0.4 mmHg (1 mmHg = 133 Pa). The duration of each experiment was ≈15–20 min. Testing of all infected erythrocytes was completed within ≈1.5 h after their removal from the controlled incubation environment.

Results and Discussion

Fabrication of Microchannels. The test channels were made of PDMS, which is a two-component silicone-based elastomer. The elastic modulus of PDMS, which can be tuned by adjusting the ratio of catalyst to elastomer, provides a good approximation of the geometric and structural properties of capillaries (29). We fabricated the microchannels to mimic capillaries between 2- and 8-μm in diameter. The average flow velocity in the central channel constriction was chosen to model the natural flow rates in capillaries (≈100–500 $\mu m \cdot s^{-1}$) (30). A schematic of the test channels is shown in Fig. 1.

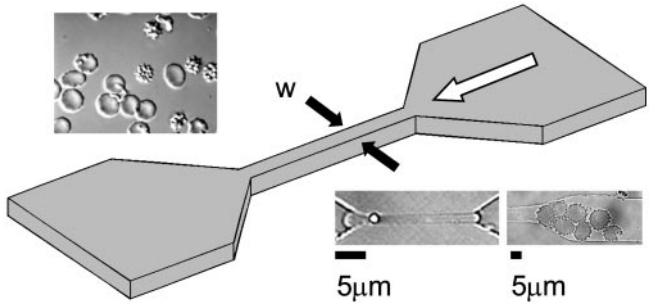

Fig. 1. Schematic illustrating the geometry of the microchannel. The constricted segment of the channel (width denoted by w) was sized at 8, 6, 4, and 2 μm. The white arrow represents the direction of fluid flow. (*Upper Inset*) A differential interference contrast image of normal (smooth) and infected RBCs. (*Lower Left Inset*) A normal RBC passing through a 2-μm constriction. (*Lower Right Inset*) Infected RBCs blocking a 6-μm constriction.

Behavior of Normal Erythrocytes. In all tests with normal erythrocytes, little or no adherence to the channel walls was observed. Furthermore, these highly flexible cells passed easily through all channel geometries, including the 2-μm constriction (see Fig. 1 *Lower Left Inset*).

Behavior of Infected Erythrocytes. To dissect out the factors that influence capillary blockage by infected erythrocytes, RBCs in different stages of infection (ring stage, early trophozoite, late trophozoite, and schizont) were passed through microchannels having different sizes of constriction (8, 6, 4, and 2 μm). Fig. 2 *A–D* shows the behavior of erythrocytes in ring-stage infection. Like normal erythrocytes, these early-stage infected cells passed through channel constrictions of all sizes with no difficulty. In contrast, early trophozoites had difficulties in passing through 4- and 2-μm channels (Fig. 2 *G* and *H*), but they could traverse 8- and 6-μm channels (Fig. 2 *E* and *F*). The first signs indicating a lack of deformability were observed in these early trophozoites. The few erythrocytes with trophozoite-stage parasites that did squeeze through the 4-μm channels did not recover their shape quickly after their passage through the constriction (Fig. 2*G*). Fig. 2 *I–L* shows the behavior of late-stage trophozoites. Similar to the early trophozoites, the late trophozoites blocked the smaller 4- and 2-μm channels (Fig. 2 *K* and *L*) but passed through larger channels with relative ease (Fig. 2 *I* and *J*). Erythrocytes in the schizont stage of infection (Fig. 2 *M–P*) exhibited a markedly increased rigidity. These cells had difficulties passing through the 6-, 4-, and 2-μm constricted channels (Fig. 2 *N–P*).

The present studies quantitatively illustrate the channel geometry in which late-stage cells cause blockage. Due to the lack of confounding factors such as ligands on endothelial cells found *in vivo*, the results obtained in our PDMS structures allow us to dissect the contributions of decreased cell deformability and membrane rigidity on movement through capillaries of precise dimensions. The stage-specific effects validate the use of microcapillaries under flow conditions to study capillary blockage.

Erythrocyte Shape Recovery. Cranston *et al.* (14) showed that, after flowing through constrictions, recovery time for ring-stage erythrocytes was significantly longer than recovery time for uninfected cells. It is believed that membrane rigidity and

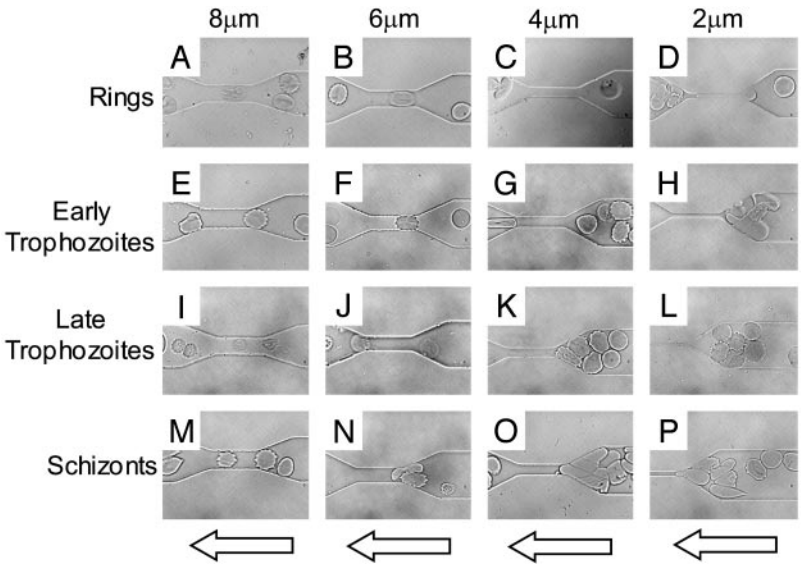

Fig. 2. Four sequences of video images of four stages of malaria-infected RBCs (early ring stage, early trophozoite, late trophozoite, and schizont) passing through channel constrictions. (*A–D*) Ring-stage infected erythrocytes retained much of the structural characteristics of normal erythrocytes and were able to pass through all constricted channels. Early trophozoite (*E–H*) and late trophozoite (*I–L*) infected cells passed through the larger 8- and 6-μm channels (*E* and *F*; *I* and *J*) but eventually blocked the smaller 4- and 2-μm channels (*G* and *H*; *K* and *L*). (*M–P*) Schizont stage infected erythrocytes blocked all but the 8-μm channel (*M*). The arrows indicate direction of flow.

internal viscosity increase as the parasite matures (2); therefore, one would expect erythrocytes in the later stages of infection to have even longer recovery times than cells in the early stages of infection. Fig. 3 shows individual erythrocytes in the early trophozoite stages of infection (Fig. 3*A*) and in the late schizont stages of infection (Fig. 3*B*) after being hydrodynamically forced through a 4-μm channel. The trophozoites generally recovered their spherical appearance within ≈30 sec. The rare schizonts that were forced through the 4-μm channel, however, did not fully recover their spherical shape even after 1–2 min of monitoring.

Pitting. Sequestering of trophozoites and schizonts under capillary flow is an important mechanism by which the parasite avoids the spleen, where efficient mechanisms exist to destroy the parasite (5, 31). Schnitzer *et al*. (31) presented *in vivo* electron micrograph evidence for the pitting of parasites from erythrocytes in the cord and sinus areas of the spleen. During pitting, the intracellular parasite is physically pushed back and eventually dissociated from the normal portion of the erythrocyte as the infected erythrocyte passes through the tiny blood vessels (cord and sinus) in the spleen. Although pitting may have complex mechanisms involving phagocytosis of the parasitic portion of the erythrocyte by a macrophage, initial separation of the parasite from the uninfected portion of the erythrocyte in the tight physical confines in the spleen are important. The product of pitting is a "ghost cell" that is free of the parasite. The parasite-free cell may be returned to circulation. Fig. 4 shows a microfluidic *in vitro* example of pitting with a 2-μm channel. Fig. 4*A Top* shows an infected cell in bright field, before passage through the restriction. Fig. 4*B Top* shows an infected cell, before the restriction, stained with 2′,7′-bis-(2-carboxyethyl)-(5 and 6)-carboxyfluorescein acetoxymethyl ester (BCECF-AM) cell stain (32). In Fig. 4*A Middle*, the normal portion of the cell is shown passing through the restriction; however, the parasitized portion of the cell remains in the upstream portion of the channel (i.e., the equivalent of the cord *in vivo*). The cell membrane continues to stretch until its ultimate load limit is exceeded and the membrane ruptures, removing the parasite from the cell. Fig. 4*B Middle* shows rupture of the membrane, an accompanying burst of fluorescence near the restriction, and separation of the parasite from the host RBC (arrow). Fig. 4*A Bottom* shows deformed cells downstream of the restriction. Fig. 4*B Bottom* shows a similar image with a fluorescent parasite (arrow) separated from the erythrocyte, which shows no further fluorescent compartments. It was common to observe ghost cells and cell debris downstream of the smaller-sized channels (e.g., 4 and 2 μm).

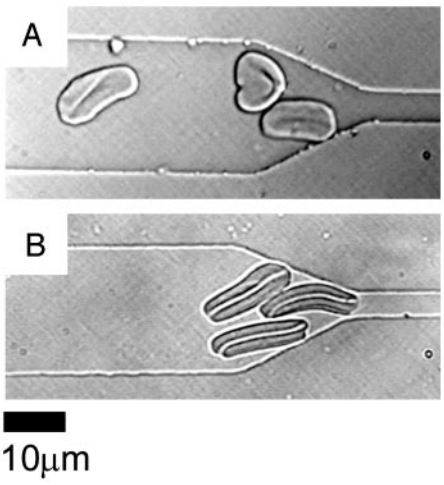

Fig. 3. Differences in recovery of compressed infected cells. (*A*) Early trophozoite stages of infected RBCs were partially distorted after passage through a 4-μm constriction and remained compressed for ≈30 sec after emerging from the channels. (*B*) Schizont forms of RBC infections were more severely deformed and did not relax back to their original shape after passage through a 4-μm constriction even 1–2 min after compression.

Normal Erythrocyte Passing Through Blockages. Fig. 5*A* shows a normal erythrocyte approaching a blockage formed by seven infected cells in the schizont stage at the entrance to the 6-μm constricted channel. The infected cells fill the entire depth of the channel near the restriction, which makes the passage above and below the blockage impossible. Rather than becoming a static part of the blockage, the normal red cell under flow conditions winds its way through the center of this group of infected cells (Fig. 5*B*). Fig. 5*C* shows the cell exiting the blockage as it enters the 6-μm channel, which it easily traverses, as was seen in Figs. 1 and 2.

The above observations have two important implications. (*i*) It is well known *in vivo*, and now also in our *in vitro* model, that

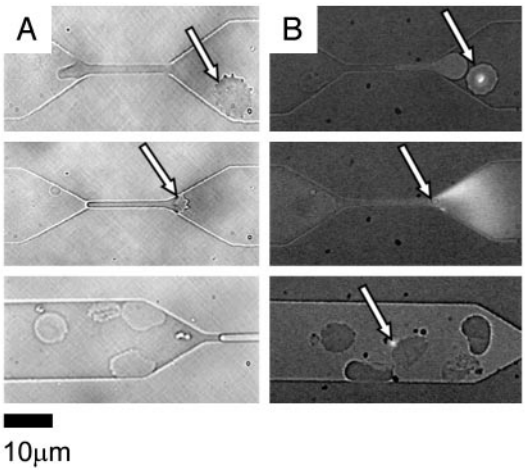

Fig. 4. Two video sequences showing pitting of infected RBCs. (*A Top*) A bright-field image shows an infected RBC before passage through a 2-μm channel (arrow). (*Middle*) The infected portion of the red cell is left outside the channel (arrow) as the rest of the red cell is squeezed through. (*Bottom*) Downstream of the constriction, note the deformed red cells and free parasites from other pitting events. (*B Top*) A fluorescent image shows a stained parasite in an infected cell before entering a channel (arrow). (*Middle*) The distal end of an infected RBC rupture (fluorescent burst) during passage through the constriction. (*Bottom*) Downstream of the constriction, note the deformed red cells and a free fluorescent parasite from another pitting event.

mature forms of infected erythrocytes concentrate to very high parasitemia at the mouth of a blocked capillary. Enrichment of parasitized cells in a growing blockage may increase local concentrations of potential malaria toxins or overstimulate host immunomodulatory responses, which contribute to pathology (33). Although the highly parasitized blockages may in part be due to cytoadherence (1, 33, 34), our model suggests that the ability of uninfected red cells to squeeze through blockages must also be important in expansion of a pathogenic blockage. (*ii*) Although exchange transfusion is known to alleviate, albeit temporarily, some of the effects of severe malaria (5), the mechanism underlying relief is not obvious. Infected cells causing pathology are unavailable for exchange because they are sequestered in capillaries, often through adherence, rosetting, and agglutination (2, 5, 33). Our experimental model shows that fresh, pliable erythrocytes can squeeze through a blockage. In a transfused patient, this action may temporarily allow delivery of nutrients and removal of toxins from distressed tissue.

Conclusions

Elastomeric microfluidic channels provide a simple, inexpensive, efficient, and accurate method to study the behavior of *P. falciparum*-infected erythrocytes under capillary-like conditions. In future research, the flexibility and cytoadherence properties of normal and infected cells can be studied by modifying the elastic modulus and the surface chemistry of PDMS microchannels. The latter will allow, under flow, controlled testing of interactions between infected erythrocytes and other RBCs, purified host cell-surface receptors, or even whole endothelial cells, owing to the high permeability of gas through PDMS. The system also provides a convenient test platform to screen potential antimalarial drugs that specifically interfere with the mechanics of infected RBCs.

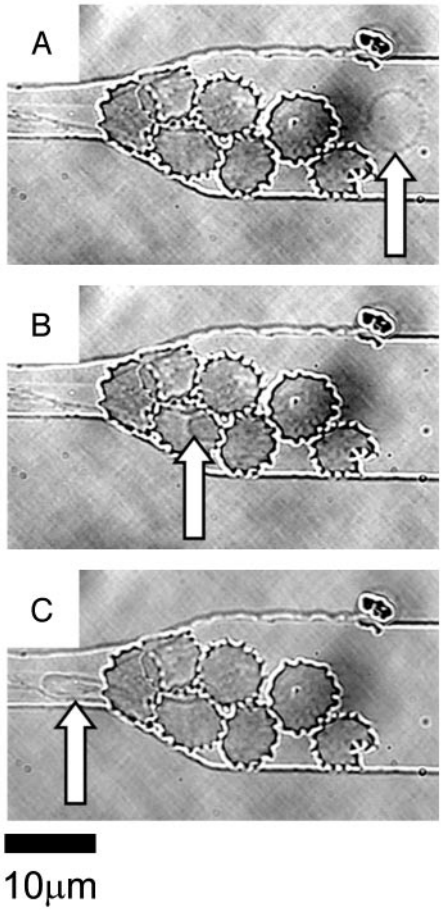

Fig. 5. A video sequence showing the passage of a normal erythrocyte through a blockage formed by infected cells. (*A*) A normal erythrocyte flows smoothly through the main channel (arrow). (*B*) The normal cell weaves its way through the blockage at the entrance to the 6-μm constriction (arrow) caused by infected RBCs in the schizont stage. (*C*) The normal cell exits the labyrinth of infected cells and passes easily through the channel constriction (arrow).

J.P.S. acknowledges support from the University of Washington Center for Nanotechnology for an Integrative Graduate Education and Research Traineeship graduate fellowship. This work was partially supported by National Institutes of Health Grants R01 AI26912 (to P.K.R.) and DA 16249 (to D.T.C.). P.K.R. is a Senior Scholar in Global Infectious Diseases from the Ellison Medical Foundation. This work also received indirect support from the Keck Foundation (University of Washington), the Bill and Melinda Gates Foundation (Seattle Biomedical Research Institute), the Dreyfus Foundation, and the Petroleum Research Fund administered by the American Chemical Society.

1. Miller, L. H., Good, M. F. & Milon, G. (1994) *Science* **264,** 1878–1883.
2. Cooke, B. M., Mohandas, N. & Coppel, R. L. (2001) *Adv. Parasitol.* **50,** 1–86.
3. World Health Organization (March 2002) *Malaria* (W.H.O., Geneva), Fact Sheet No. 94.
4. Evans, E. (1989) *Methods Enzymol.* **173,** 3–35.
5. Dondorp, A. M., Kager, P. A., Vreeken, J. & White, N. J. (2000) *Parasitol. Today* **16,** 228–232.
6. Stuart, J. (1985) *J. Clin. Pathol.* **38,** 965–977.
7. Miller, L. H., Usami, S. & Chien, S. (1971) *J. Clin. Invest.* **50,** 1451–1455.
8. Miller, L. H., Chien, S. & Usami, S. (1972) *Am. J. Trop. Med. Hyg.* **21,** 133–136.
9. Areekul, S. & Yamarat, P. (1988) *J. Med. Assoc. Thailand* **71,** 196–202.
10. Bessis, M. & Mohandas, N. A. (1975) *Blood Cells* **1,** 307–313.
11. Kiesenwetter, H., Dauer, U., Teitel, P., Schmid-Schonbein, H. & Trapp, R. (1982) *Biorheology* **19,** 737–753.
12. Roggenkamp, H. G., Jung, F., Schneider, R. & Kiesewetter, H. (1984) *Biorheology Suppl.* **1,** 241–243.
13. Fischer, T. M., Stöhr-Liesen, M. & Schmid-Schönbein, H. (1978) *Science* **202,** 894–896.

14. Cranston, H. A., Boylan, C. W., Carroll, G. L., Sutera, S. P., Williamson, J. R., Gluzman, I. Y. & Krogstad, D. J. (1984) *Science* **223,** 400–403.
15. Nash, G. B., O'Brien, E., Gordon, S. E. & Dormandy, J. A. (1989) *Blood* **74,** 855–861.
16. Paulitschke, M. & Nash, G. B. (1993). *J. Lab. Clin. Med.* **122,** 581–589.
17. Whitesides, G. M., Ostuni, E., Shuichi, T., Jiang, X. & Ingber, D. E. (2001) *Annu. Rev. Biomed. Eng.* **3,** 335–373.
18. Voldman, J., Gray, M. L. & Schmidt, M. A. (1999) *Annu. Rev. Biomed. Eng.* **1,** 401–425.
19. Wilding, P., Pfahler, J., Bau, H. H., Zemel, J. N. & Kricka, L. J. (1994) *Clin. Chem.* **40,** 43–47.
20. Tracey, M. C., Greenaway, R. S., Das, A., Kaye, P. H. & Barnes, A. J. (1995) *IEEE Trans. Biomed. Eng.* **42,** 751–761.
21. Brody, J. P., Han, Y., Austin, R. H. & Bitensky, M. (1995) *Biophys. J.* **68,** 2224–2232.
22. Sutton, N., Tracey, M. C., Johnston, I. D., Greenaway, R. S. & Rampling, M. W (1997) *Microvasc. Res.* **53,** 272–281.
23. Cokelet, G. R., Soave, R., Pugh, G. & Rathbun, L. (1993) *Microvasc. Res.* **46,** 394–400.
24. Gifford, C. S., Frank, M. G., Derganc, J., Gabel, C., Austin, R. H., Yoshida, T. & Bitensky, M. W. (2003) *Biophys. J.* **84,** 623–633.
25. McDonald, J. C., Duffy, D. C., Anderson, J. R., Chiu, D. T., Wu, H., Schueller, O. J. A. & Whitesides, G. M (2000). *Electrophoresis* **21,** 27–40.
26. Trager, W. & Jensen, J. B. (1976) *Science* **193,** 673–675.
27. Schuster, F. L. (2002) *Clin. Microbiol. Rev.* **15,** 355–364.
28. Wissing, F., Sanchez, C., Rohrbach, P., Ricken, S. & Lanzer, M. (2002) *J. Biol. Chem.* **277,** 37747–37755.
29. McDonald, J. C. & Whitesides, G. M. (2002) *Acc. Chem. Res.* **35,** 491–499.
30. Shelby, J. P. & Chiu, D. T. (2003) *Anal. Chem.* **75,** 1387–1392.
31. Schnitzer, B., Sodeman, T. & Mead, M. L. (1972) *Science* **177,** 175–177.
32. Hayashi, M., Yamada, H., Mitamura, T., Horii, T., Yamamoto, A. & Moriyama, Y. (2000) *J. Biol. Chem.* **275,** 34353–34358.
33. Miller, L. H., Baruch, D. I., Marsh, K. & Doumbo, O. K. (2002) *Nature* **415,** 673–679.
34. Crabb, B. S., Cooke, B. M., Reeder, J. C., Waller, R. F., Caruana, S. R., Davern, K. M., Wickham, M. E., Brown, G. V., Coppel, R. L. & Cowman, A. F. (1997) *Cell* **89,** 287–296.